PHYSICAL REVIEW B **92**, 020414(R) (2015)

Comparison of the magneto-Peltier and magneto-Seebeck effects in magnetic tunnel junctions

J. Shan,[1,*] F. K. Dejene,[1] J. C. Leutenantsmeyer,[1] J. Flipse,[1] M. Münzenberg,[2] and B. J. van Wees[1]

[1]*Physics of Nanodevices, Zernike Institute for Advanced Materials, University of Groningen, Nijenborgh 4, 9747 AG Groningen, The Netherlands*

[2]*Institut für Physik, Greifswald University, Felix-Hausdorff-Strasse 6, 17489 Greifswald, Germany*

(Received 28 May 2015; revised manuscript received 6 July 2015; published 28 July 2015)

Understanding heat generation and transport processes in a magnetic tunnel junction (MTJ) is a significant step towards improving its application in current memory devices. Recent work has experimentally demonstrated the magneto-Seebeck effect in MTJs, where the Seebeck coefficient of the junction varies as the magnetic configuration changes from a parallel (P) to an antiparallel (AP) configuration. Here we report a study on its reciprocal effect, the magneto-Peltier effect, where the heat flow carried by the tunneling electrons is altered by changing the magnetic configuration of the MTJ. The magneto-Peltier signal that reflects the change in the temperature difference across the junction between the P and AP configurations scales linearly with the applied current in the small bias but is greatly enhanced in the large-bias regime, due to higher-order Joule heating mechanisms. By carefully extracting the linear response which reflects the magneto-Peltier effect, and comparing it with the magneto-Seebeck measurements performed on the same device, we observe results consistent with Onsager reciprocity. We estimate a magneto-Peltier coefficient of 13.4 mV in the linear regime using a three-dimensional thermoelectric model. Our result opens up the possibility of programmable thermoelectric devices based on the Peltier effect in MTJs.

DOI: 10.1103/PhysRevB.92.020414 PACS number(s): 85.80.Fi, 85.75.Dd, 72.25.−b

The electrical resistance of a magnetic tunnel junction (MTJ), a stack of two ferromagnetic layers separated by an insulating tunnel barrier, depends on the relative magnetic orientation of the two magnetic layers [1–3]. This tunnel magnetoresistance (TMR) effect puts MTJs at the forefront of the applications in the field of spintronics [4]. Spin caloritronics [5–7] is an emerging field that couples thermoelectric effects with spintronics. Many interesting physical phenomena were discovered such as the spin(-dependent) Seebeck effect in magnetic metals [8], magnetic semiconductors [9], and magnetic insulators [10]. Particularly, in spin tunneling devices, the magneto-Seebeck effect was theoretically studied [11–14] and experimentally observed [15–20] in MTJs, where the Seebeck coefficient of the junction can be varied by changing the magnetic configuration. More recently, the spin(-dependent) Peltier effect that is driven by spin(-polarized) currents has been experimentally observed in metallic [21,22] and insulating ferromagnets [23], which are shown to obey the Thomson-Onsager reciprocity relation [24–26] to the spin (-dependent) Seebeck effect. From this relation, the reciprocal effect of the magneto-Seebeck effect, which can be called the magneto-Peltier effect, is also expected in MTJs [see Figs. 1(a) and 1(b)].

However, experimental studies of the magneto-Peltier effect are lacking. Its small effect compared to the often-dominant Joule heating effects has left the experimental observation elusive. In this Rapid Communication, we report an experimental study of the magneto-Peltier effect as well as higher-order heating effects, and compare the Peltier measurements to the Seebeck measurements on the same junction. Via sensitive thermometry architecture and measurement techniques, we are able to measure small temperature changes as well as distinguish between the linear (due to Peltier effect) and nonlinear effects (due to Joule heating).

Although both the electric conductance and Seebeck coefficient depend on the relative magnetic configuration in an MTJ, the mechanisms behind them are not the same. While the electric conductance is determined by the transmission probability $T_{\mathrm{P,AP}}(E)$ of electrons across the insulating barrier around the Fermi energy E_F, the Seebeck coefficient $S_{\mathrm{P,AP}}$ solely depends on the electron-hole asymmetry of $T_{\mathrm{P,AP}}(E)$ around E_F. By Onsager reciprocity, the Peltier coefficient Π is closely related to S by $\Pi = ST_0$, where T_0 denotes certain temperature. Using the expression for S [11,15] we can express Π as

$$\Pi_{\mathrm{P,AP}} = -\frac{\int T_{\mathrm{P,AP}}(E)(E - E_F)(-\partial_E f_0)dE}{e\int T_{\mathrm{P,AP}}(E)(-\partial_E f_0)dE}, \qquad (1)$$

where e is the elementary charge and f_0 is the Fermi-Dirac distribution function at temperature T_0. For a constant tunneling current I through the MTJ, the Peltier heat Q_Π carried by this current is different for the P and AP configurations, leading to different temperature biases across the junction between the two configurations. Disregarding Joule heating, the temperature difference between the parallel and antiparallel configuration $\Delta T = \Delta T_{\mathrm{AP}} - \Delta T_{\mathrm{P}}$ can be estimated by balancing the Peltier heat Q_Π with the backflow of the heat current through the junction as

$$\Delta T = \frac{tI}{\kappa_{\mathrm{MgO}}A}(\Pi_{\mathrm{AP}} - \Pi_{\mathrm{P}}), \qquad (2)$$

where t is the thickness of the tunnel barrier, κ_{MgO} is the thermal conductivity of the MgO layer [27], and A is the area of the junction. Using the parameters given in Ref. [15], it can be estimated that for an electric current density of $5 \times 10^3 \mathrm{A/cm}^2$ through the junction, the change in temperature due to the magneto-Peltier effect can reach $\sim 100\,\mu\mathrm{K}$ at

*j.shan@rug.nl

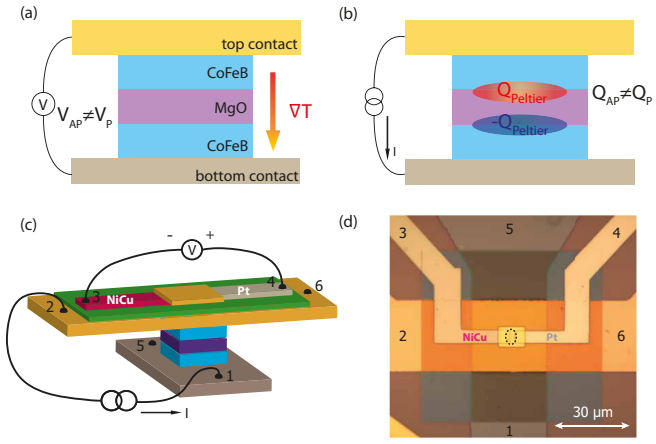

FIG. 1. (Color online) Concept and device geometry. (a) Concept of the magneto-Seebeck effect. A temperature gradient is applied across an MTJ, resulting in a Seebeck voltage that is dependent on the magnetic configuration. (b) Concept of the magneto-Peltier effect. A charge current is sent through an MTJ, resulting in a Peltier heating/cooling at the interfaces that also depends on the magnetic configuration. Joule heating is not shown for simplicity. (c) Schematic representation of the measured device. A Pt-NiCu (constantan) thermocouple that is electrically isolated from the top contact by an Al_2O_3 layer (green color) is used to detect temperature changes. In the Peltier measurement, charge current is sent through the pillar (from contact 1 to 2), while recording the voltage over the thermocouple (contacts 3 and 4), as plotted here. Contacts 5 and 6 are used for four-probe TMR measurements. For the reciprocal Seebeck measurement, current is sent through the thermocouple while recording the voltage over the pillar using contacts 1 and 2. (d) Optical microscope image of the measured device. The dotted circle indicates the location of the MTJ. The size of the junction measured in the main text is $2.7 \times 5\ \mu\text{m}^2$ by size.

room temperature, which requires a sensitive thermometry technique, as we use here.

Figures 1(c) and 1(d) show the device geometry and measurement configuration as employed in our experiment. We study the CoFeB/MgO/CoFeB MTJs, the same as in Ref. [15], that are reported to have a large magneto-Seebeck effect [11,15,16] due to their half-metallic transmission property [3]. The layer structure of the patterned MTJ sample stack (from bottom to top) is Si (100)/SiO_2 500 nm/Ta 15 nm/CoFeB 2.5 nm/MgO 2.1 nm/CoFeB 5.4 nm/Ta 5 nm/Ru 3 nm/Cr 5 nm/Au 25 nm. Detailed fabrication processes can be found in Ref. [15]. To sense the temperature change locally at the top of the junction, a thermocouple consisting of constantan ($Ni_{45}Cu_{55}$) and Pt is fabricated over the top contact of the MTJ [22,25,28]. Constantan is dc sputtered and Pt is *e*-beam evaporated, both 90 nm in thickness. A 50-nm-thick Al_2O_3 layer is *e*-beam evaporated over the top contact to electrically isolate MTJ and thermocouple from the top contact, so that no charge-related effects are picked up by the thermocouple. Finally, an 130-nm layer of Au is deposited to connect the two arms of thermocouple, creating a uniform temperature distribution over the junction. In the Peltier measurement configuration, we send a charge current through the pillar (contact 1 to 2) while recording the thermovoltage using the thermocouple (contact 3 to 4). Note that in this configuration the temperature changes resulting from both the Peltier and Joule heating effects are measured. Meanwhile we also record the tunnel magnetoresistance (TMR) by a four-probe method using contacts 5 and 6. All measurements shown in the main text are performed on a single device at room temperature. Measurements on two other samples can be found in Supplemental Material Sec. 1 [29].

A standard lock-in technique is used for our measurements, where an ac current (with an rms value of I_0) is sent through the system at a low excitation frequency (∼17 Hz), so that a steady-state temperature condition is reached and at the same time capacitive coupling is suppressed. The voltage output from the sample is separated into different harmonic signals ($V^{1f}, \ldots, V^{nf}$) in terms of the input frequency. With this technique it is possible to isolate the Peltier effect that is linear with current from the Joule heating effect that is of second or even higher responses. In a simple case where only V^{1f} and V^{2f} are present, the first-order response ($R_1 I_0$, such as the Peltier effect) is linked to V^{1f} while the second-order response ($R_2 I_0^2$, such as the Joule heating effect) is linked to V^{2f}. But in a more complex case where higher-order effects are also present [25,30], the nth-order response ($R_n I_0^n$) is not directly equal to the nth harmonic signal (V^{nf}); instead, all higher harmonic signals (with the same parity as n) that are nonzero need to be included by a straightforward algebraic operation, for instance,

$$R_1 I_0 = \sum_{\text{odd } n} n V^{nf}. \tag{3}$$

So we can calculate the linear response from different harmonic signals (see Supplemental Material Sec. 2 [29] for details).

Figure 2 shows the experimental results of the magneto-Peltier measurements. We apply an ac current of 150 μA (rms) through the MTJ while sweeping the magnetic field. Both the first and second harmonic voltages recorded at the thermocouple (V^{1f} and V^{2f}), shown in Figs. 2(a) and 2(b), exhibit four abrupt changes corresponding to the switching from P to AP configuration and back, implying a change in the temperature at the top contact. V^{1f} of TMR is shown in Fig. 2(c). We measure the current dependence of these signals correspondingly, for both the P and AP configurations, as shown in Figs. 2(d)–2(f). We did not apply ac currents higher than 150 μA to avoid a dielectric breakdown of the MTJ (∼2 V across the junction for 2.1 nm MgO) [31]. In the P configuration we have a simple case where no higher harmonic signals can be detected, and the V^{1f} (V^{2f}) signal detected at the thermocouple is linear (quadratic) with the current, which can be considered as the Peltier signal (Joule heating signal). However, for the AP configuration, we have a more complex case where higher-order effects are present. The I-V characteristic of the MTJ (see Supplemental Material Sec. 4 [29]) is nonlinear with the current in contrast to the linear behavior in the P configuration [32]; in other words, the resistance of the junction R is bias dependent for AP [33–35]. Therefore, the Joule heating effect (IV) is not only present in the second order, but also brings on higher-order responses. The consequence of this nonlinearity is twofold: First, R decreases with both larger positive and negative biases. This

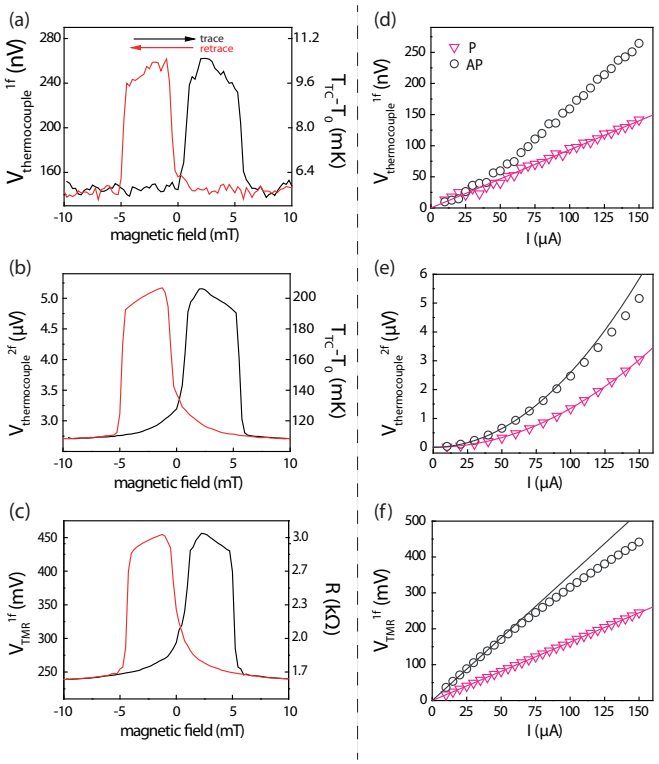

FIG. 2. (Color online) Lock-in signals from magneto-Peltier and TMR measurement configurations. (a), (b) First (V^{1f}) and second (V^{2f}) harmonic signal measured at the thermocouple for an rms current of 150 μA. (c) First (V^{1f}) harmonic signal of TMR measured at the same current. On the right axes the temperature differences detected by the thermocouple relative to the room temperature T_0 are given as $T_{TC} - T_0 = V^{1f(2f)}/(S_{Pt} - S_{NiCu})$, where T_0 is 290 K. (d)–(f) Current dependence of the corresponding measurements, for P (open triangles) and AP (open circles) configurations, where P (AP) is obtained when setting the magnetic field at 10 (2) mT. Solid lines are linear [in (d) and (f)] or quadratic fits [in (e)], as references.

leads to even higher-order responses at the thermocouple which deviate the V^{2f} from a quadratic behavior, as shown in Fig. 2(e). Second, R also shows an asymmetric dependence for $+I$ and $-I$, i.e., $V(+I) \neq -V(-I)$, indicating that the dissipation at the junction is different when the bias is reversed. The reason for this asymmetry can be attributed to the inevitable difference between the two interfaces across the MgO [35,36]. Although this effect is only present in higher odd order heating signals on thermocouple, it mimics a Peltier-like effect and strongly deviates V^{1f} from a linear behavior [see Fig. 2(d)]. A more extensive quantitative analysis can be found in Supplemental Material Sec. 4 [29].

It is therefore important to determine the pure linear signal ($R_1 I_0$) of the AP case in order to discuss the magneto-Peltier effect. Taking advantage of the lock-in detection technique, we can measure the higher harmonic signals ($V^{3f}, V^{5f}, \ldots$) by tuning the lock-in detection frequency to the corresponding harmonics frequency. The first-order (linear) response can be obtained using Eq. (3). Here we only include higher harmonic signals up to V^{5f}, as V^{7f} cannot be determined accurately within our noise level ($\leqslant$|5 nV|). The results are shown in Fig. 3(a). However, the difference between P and AP still shows a seventh-order behavior as a function of the current. This means that, especially at larger currents (above 80 μA), the seventh-order response is still present; however, the V^{7f} signal that can be measured is only 1/8 of the seventh-order response, which made it difficult to be included to extract $R_1 I_0$. Nevertheless, we can still rely on the lower-current regime before the onset of the seventh-order response [below 80 μA, the circled part in Fig. 3(a)], which can be regarded as a purely linear regime. We fit the curves for P and AP individually for this regime and especially focus on their difference, which can be considered as the magneto-Peltier effect. Although the difference is small compared to the noise, we fit it linearly and estimate a slope range bounded by one standard deviation, 58 ± 35 $\mu\Omega$, as shown in the inset of Fig. 3(b).

To support our estimation of the magneto-Peltier signal, we perform magneto-Seebeck measurements on the same device by effectively reversing the role of the current and voltage contacts as used in the Peltier measurement. Here we send an ac current through the thermocouple (contact 3 to 4) thereby creating a vertical temperature gradient over the MTJ via the Peltier heating/cooling ($\propto I$) at the NiCu-Au and Au-Pt interfaces. The Seebeck voltage (open-circuit thermovoltage) due to this vertical temperature gradient is measured using contacts 1 to 2. In Seebeck measurements, it is possible to send larger currents up to 2 mA through the thermocouple with a resistance of 190 Ω. Unlike the Peltier measurement, in the Seebeck measurement no higher odd harmonic features are observed for either P or AP configurations, implying a linear behavior for the Seebeck signal in the measured current range. This is because the thermocouple is purely ohmic, in contrast to the nonlinear MTJ. The current dependences of the magneto-Seebeck measurements are shown in Fig. 3(c). According to the Thomson-Onsager reciprocity relation, the linear response signals for the Peltier and Seebeck effect should be the same, as well as the difference between P and AP configurations [25]. From Fig. 3(c), the difference between the two configurations is 12.5 ± 0.4 $\mu\Omega$, which falls into the estimated range of the magneto-Peltier effect within two standard deviations (corresponding to a confidence level of 95%), therefore showing no statistically significant difference. This is consistent with the reciprocity between the magneto-Seebeck and magneto-Peltier measurements. In our opinion, there is no fundamental reason for the rather large difference in the average values for magneto-Peltier and Seebeck coefficients, except for the experimental difficulties in obtaining the magneto-Peltier coefficient. Note that the background signals for Seebeck and Peltier configurations correspond closely, indicating the validity of our approach. However, the backgrounds contain Seebeck or Peltier effects from all metal interfaces, and therefore are not directly linked to the Seebeck or Peltier coefficients of the MTJ.

By using a three-dimensional finite element model (3D-FEM) [37] we can quantify our results. We focus on the estimation of the relative change of the Peltier coefficient from the P to AP configuration of the MTJ. We do not model the electron tunneling process, but regard MgO as a conductor whose electrical conductivity and Peltier coefficient vary between P and AP states, while keeping other properties of the MTJ constant. The details can be found in Supplemental

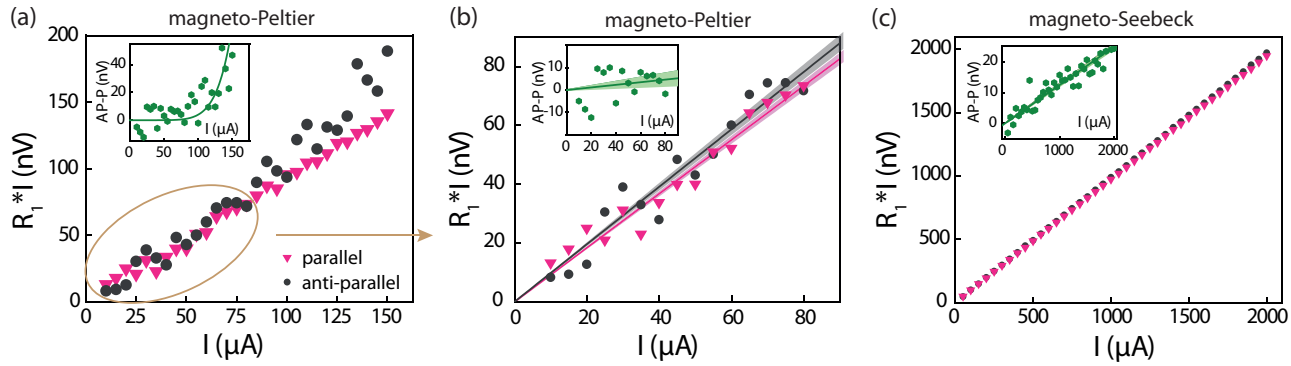

FIG. 3. (Color online) Comparison of the magneto-Peltier and magneto-Seebeck linear responses. (a) The extracted linear response calculated up to including the V^{5f}, as a function of applied current. The circled part is where the V^{7f} is close to 0 and is therefore represents pure linear signals. The inset shows the difference between the P and AP configurations which is fitted to a seventh-order behavior. (b) Linear fitting of the circled part in (a). The shaded zones indicate the standard deviations of the fitted slopes. The inset shows the difference between the P and AP configurations which is linearly fitted, with the shaded area indicating one standard deviation. (c) Current dependence of the Seebeck measurements, without any compensations from higher harmonic signals. The inset shows the difference between the AP and P configurations which is fitted to a linear behavior.

Material Sec. 3 [29]. We find that the modeled magneto-Peltier signal is very sensitive to the choice of κ_{MgO}, and the difficulty of measuring this quantity directly can create a big uncertainty in our estimation. Here we adopt the same value from Ref. [15], where $\kappa_{\mathrm{MgO}} = 4$ W/(m K) was used for the 2.1-nm MgO layer, taking into account both the crystalline quality of MgO and its thermal interfaces with CoFeB. By fitting to our experimental result 12.5 ± 0.4 $\mu\Omega$ from the Seebeck measurements (which has less statistical uncertainty), we obtain the change of the Peltier coefficient of MgO to be $\Delta\Pi = \Pi_{\mathrm{AP}} - \Pi_{\mathrm{P}} = \Delta S T = 13.4$ mV from P to AP, which by the Onsager relation corresponds to $\Delta S = S_{\mathrm{AP}} - S_{\mathrm{P}} = 46.2$ μV/K. This is close to the Seebeck coefficient change of MgO reported in Ref. [15]. Note that κ_{MgO} could actually be smaller, as recently suggested by Zhang *et al.* from *ab initio* calculations [38]. In that case, $\Delta\Pi$ would be proportionally lower.

In conclusion, we have observed the magneto-Peltier effect in magnetic tunnel junctions and confirmed its reciprocity to the magneto-Seebeck effect by measuring both effects in a single device. We also observed higher-order heating effects which greatly enhance the magneto-Peltier signal in the large-bias regime. We attribute this effect to the asymmetric resistance of MTJ for the opposite bias. In addition to providing additional insight in the nature of heat dissipation in MTJs, our results open up the possibility of a magnetically controllable cooling mechanism in MTJs, which can be potentially applied in magnetic logic devices. We anticipate that the magneto-Peltier effect could be further increased in lower resistance junctions with a larger contrast of the electron-hole asymmetry of $T(E)$ between the P and AP configurations, perhaps in optimized material systems.

The authors thank G. Reiss and T. Kuschel for helpful discussions, M. Walter for MTJ growth parameter optimization, and M. de Roosz, H. Adema, T. Schouten, and J. G. Holstein for technical assistance. This work is part of the research program of the Foundation for Fundamental Research on Matter (FOM) and is supported by NanoLab NL, the priority program DFG SpinCaT 1538 within MU 1780/8-1,2, EU-FET Grant InSpin 612759, and the Zernike Institute for Advanced Materials.

J.S. and F.K.D. contributed equally to this work.

[1] T. Miyazaki and N. Tezuka, J. Magn. Magn. Mater. **139**, L231 (1995).

[2] S. S. P. Parkin, C. Kaiser, A. Panchula, P. M. Rice, B. Hughes, M. Samant, and S.-H. Yang, Nat. Mater. **3**, 862 (2004).

[3] S. Yuasa, T. Nagahama, A. Fukushima, Y. Suzuki, and K. Ando, Nat. Mater. **3**, 868 (2004).

[4] I. Žutić, J. Fabian, and S. Das Sarma, Rev. Mod. Phys. **76**, 323 (2004).

[5] G. E. W. Bauer, A. H. MacDonald, and S. Maekawa, Solid State Commun. **150**, 459 (2010).

[6] G. E. W. Bauer, E. Saitoh, and B. J. van Wees, Nat. Mater. **11**, 391 (2012).

[7] S. R. Boona, R. C. Myers, and J. P. Heremans, Energy Environ. Sci. **7**, 885 (2014).

[8] A. Slachter, F. L. Bakker, J.-P. Adam, and B. J. van Wees, Nat. Phys. **6**, 879 (2010).

[9] C. M. Jaworski, J. Yang, S. Mack, D. D. Awschalom, J. P. Heremans, and R. C. Myers, Nat. Mater. **9**, 898 (2010).

[10] K. Uchida, J. Xiao, H. Adachi, J. Ohe, S. Takahashi, J. Ieda, T. Ota, Y. Kajiwara, H. Umezawa, H. Kawai, G. E. W. Bauer, S. Maekawa, and E. Saitoh, Nat. Mater. **9**, 894 (2010).

[11] M. Czerner, M. Bachmann, and C. Heiliger, Phys. Rev. B **83**, 132405 (2011).

[12] C. Heiliger, C. Franz, and M. Czerner, Phys. Rev. B **87**, 224412 (2013).

[13] S.-Z. Wang, K. Xia, and G. E. W. Bauer, Phys. Rev. B **90**, 224406 (2014).

[14] C. López-Monís, A. Matos-Abiague, and J. Fabian, Phys. Rev. B **89**, 054419 (2014).

[15] M. Walter, J. Walowski, V. Zbarsky, M. Münzenberg, M. Schäfers, D. Ebke, G. Reiss, A. Thomas, P. Peretzki,

M. Seibt, J. S. Moodera, M. Czerner, M. Bachmann, and C. Heiliger, Nat. Mater. **10**, 742 (2011).

[16] N. Liebing, S. Serrano-Guisan, K. Rott, G. Reiss, J. Langer, B. Ocker, and H. W. Schumacher, Phys. Rev. Lett. **107**, 177201 (2011).

[17] W. Lin, M. Hehn, L. Chaput, B. Negulescu, S. Andrieu, F. Montaigne, and S. Mangin, Nat. Commun. **3**, 744 (2012).

[18] Z. H. Zhang, Y. S. Gui, L. Fu, X. L. Fan, J. W. Cao, D. S. Xue, P. P. Freitas, D. Houssameddine, S. Hemour, K. Wu, and C.-M. Hu, Phys. Rev. Lett. **109**, 037206 (2012).

[19] J. M. Teixeira, J. D. Costa, J. Ventura, M. P. Fernandez-Garcia, J. Azevedo, J. P. Araujo, J. B. Sousa, P. Wisniowski, S. Cardoso, and P. P. Freitas, Appl. Phys. Lett. **102**, 212413 (2013).

[20] A. Boehnke, M. Milnikel, M. von der Ehe, C. Franz, V. Zbarsky, M. Czerner, K. Rott, A. Thomas, C. Heiliger, G. Reiss, and M. Münzenberg, Sci. Rep. **5**, 8945 (2015).

[21] L. Gravier, S. Serrano-Guisan, F. Reuse, and J.-P. Ansermet, Phys. Rev. B **73**, 052410 (2006).

[22] J. Flipse, F. L. Bakker, A. Slachter, F. K. Dejene, and B. J. van Wees, Nat. Nanotechnol. **7**, 166 (2012).

[23] J. Flipse, F. K. Dejene, D. Wagenaar, G. E. W. Bauer, J. B. Youssef, and B. J. van Wees, Phys. Rev. Lett. **113**, 027601 (2014).

[24] L. Onsager, Phys. Rev. **37**, 405 (1931).

[25] F. K. Dejene, J. Flipse, and B. J. van Wees, Phys. Rev. B **90**, 180402 (2014).

[26] A. D. Avery and B. L. Zink, Phys. Rev. Lett. **111**, 126602 (2013).

[27] The κ_{MgO} can be assumed to be independent of the magnetic configuration, since the thermal transport through MgO is dominated by phonons (κ_{ph}) instead of electrons (κ_e), given the thickness of the MgO we used (10 monolayers) [38]. In contrast to κ_e, κ_{ph} is not sensitive to the magnetic configuration.

[28] F. K. Dejene, J. Flipse, G. E. W. Bauer, and B. J. van Wees, Nat. Phys. **9**, 636 (2013).

[29] See Supplemental Material at http://link.aps.org/supplemental/10.1103/PhysRevB.92.020414 for results of other samples, descriptions of lock-in detection technique, details of 3D finite modeling, and a quantitative analysis of higher order Joule heating effects.

[30] N. Vlietstra, J. Shan, B. J. van Wees, M. Isasa, F. Casanova, and J. Ben Youssef, Phys. Rev. B **90**, 174436 (2014).

[31] A. A. Khan, J. Schmalhorst, A. Thomas, O. Schebaum, and G. Reiss, J. Appl. Phys. **103**, 123705 (2008).

[32] G. X. Miao, Y. J. Park, J. S. Moodera, M. Seibt, G. Eilers, and M. Münzenberg, Phys. Rev. Lett. **100**, 246803 (2008).

[33] J. S. Moodera, L. R. Kinder, T. M. Wong, and R. Meservey, Phys. Rev. Lett. **74**, 3273 (1995).

[34] S. Zhang, P. M. Levy, A. C. Marley, and S. S. P. Parkin, Phys. Rev. Lett. **79**, 3744 (1997).

[35] S. O. Valenzuela, D. J. Monsma, C. M. Marcus, V. Narayanamurti, and M. Tinkham, Phys. Rev. Lett. **94**, 196601 (2005).

[36] C. Heiliger, P. Zahn, B. Y. Yavorsky, and I. Mertig, Phys. Rev. B **73**, 214441 (2006).

[37] A. Slachter, F. L. Bakker, and B. J. van Wees, Phys. Rev. B **84**, 174408 (2011).

[38] J. Zhang, M. Bachman, M. Czerner, and C. Heiliger, Phys. Rev. Lett. **115**, 037203 (2015).